A review on recent advances in selective and sensitive detection of heavy toxic metal ions in water using g-C_3N_4-based heterostructured composites

Dasari Ayodhya*

Department of Chemistry, University College of Science, Osmania University, Hyderabad-500007, Telangana State, India

Corresponding author information:

*E-mail: ayodhyadasari@gmail.com; ayodyadasari@osmania.ac.in

Tel: +91 9010877323

Supplementary information

Figures

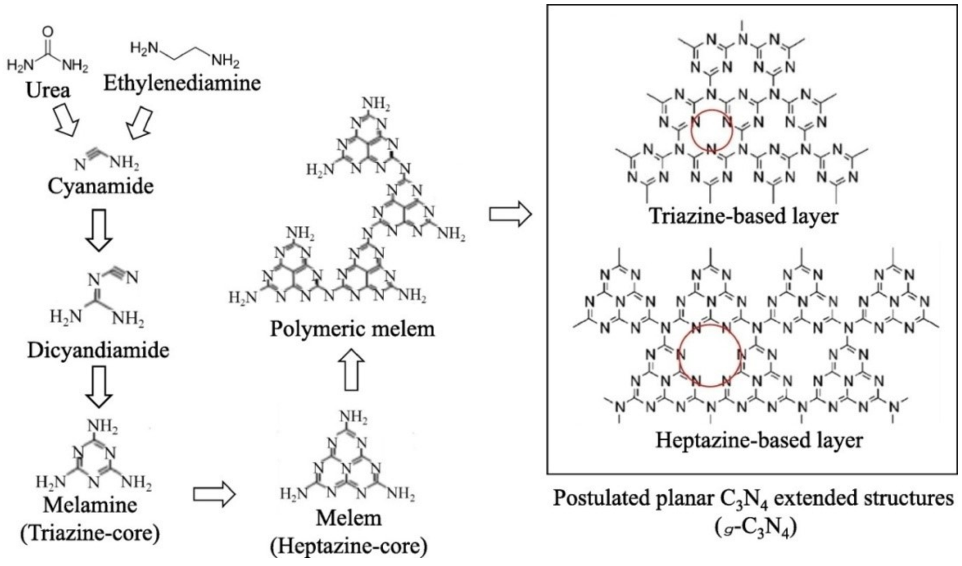

Fig. S1 Structural evolution from urea and ethylenediamine to g-C_3N_4, Characteristic intrinsic vacancies surrounded by nitrogen atoms are emphasized by red circles.[43]

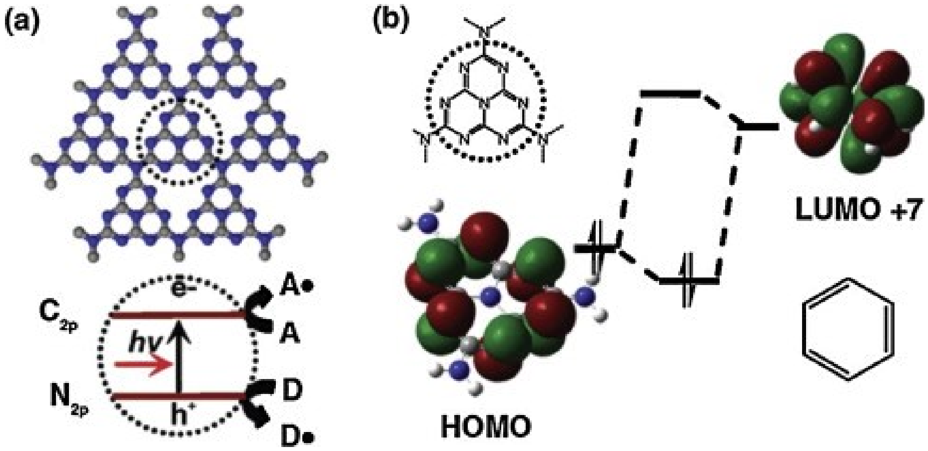

Fig. S2 (a) Stacked g-C_3N_4 sheets function as an all-organic solid-statephotocatalyst promoting redox reactions with visible light; (b) chemical interaction of benzene and defective g-C_3N_4 via HOMO–LUMO hybridization of melem and benzene.[27]

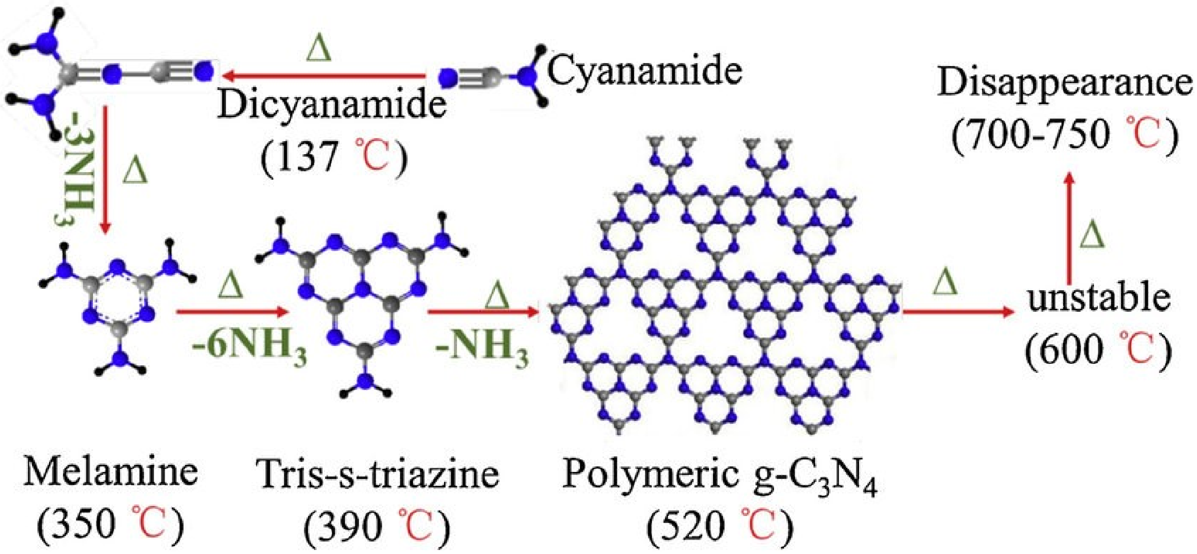

Fig. S3 Reaction path for the formation of g-C_3N_4 starting from cyanamide.[51]

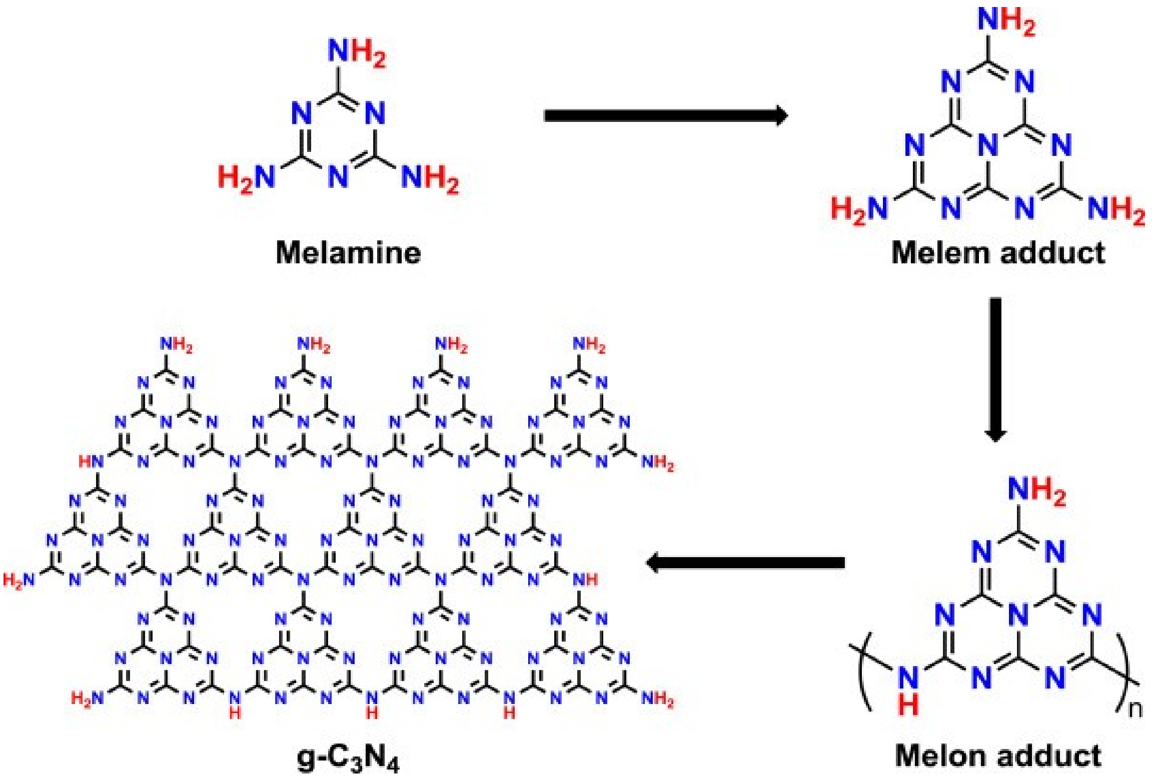

Fig. S4 Reaction pathway for the formation of g-C_3N_4 by polycondensation of Melamine.[64]

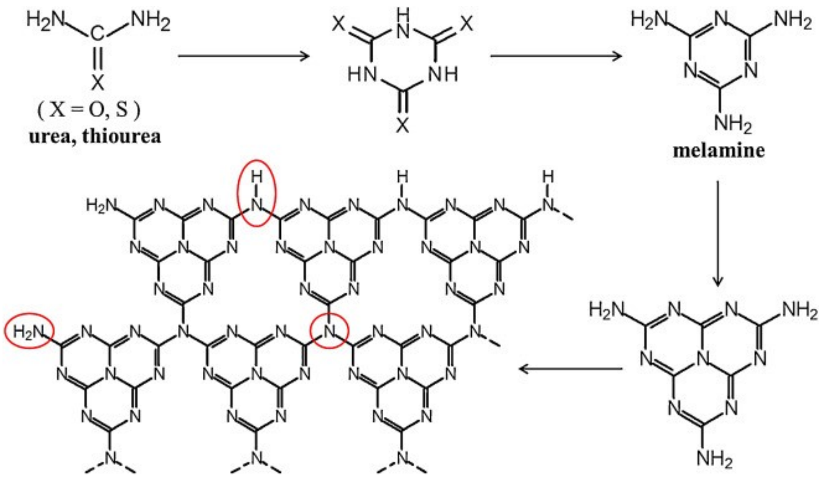

Fig. S5 Reaction paths for the formation of g-C_3N_4 from melamine, thiourea, and urea.[65]

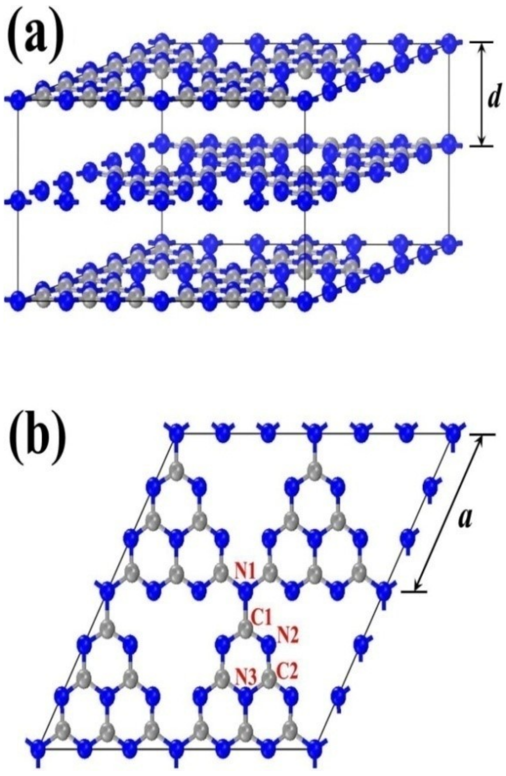

Fig. S6 Geometric structures of (a) bulk g-C_3N_4 and (b) single layer g-C_3N_4; the gray and blue balls are carbon and nitrogen atoms, respectively.[67]

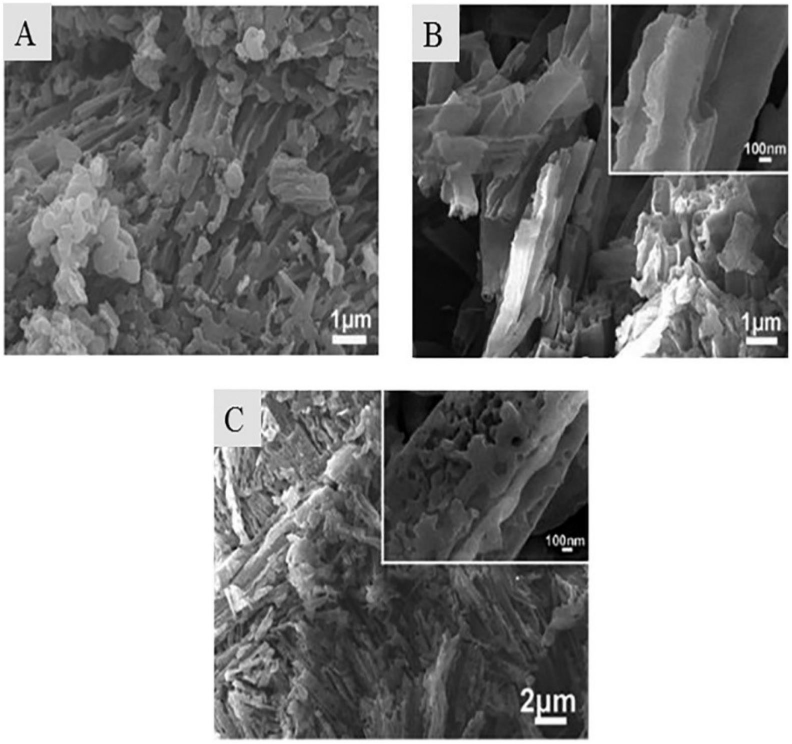

Fig. S7 SEM images of g-C_3N_4 with different morphology. (A) nanoflakes, (B) nanotubes, (C) rod-like structure.[74]

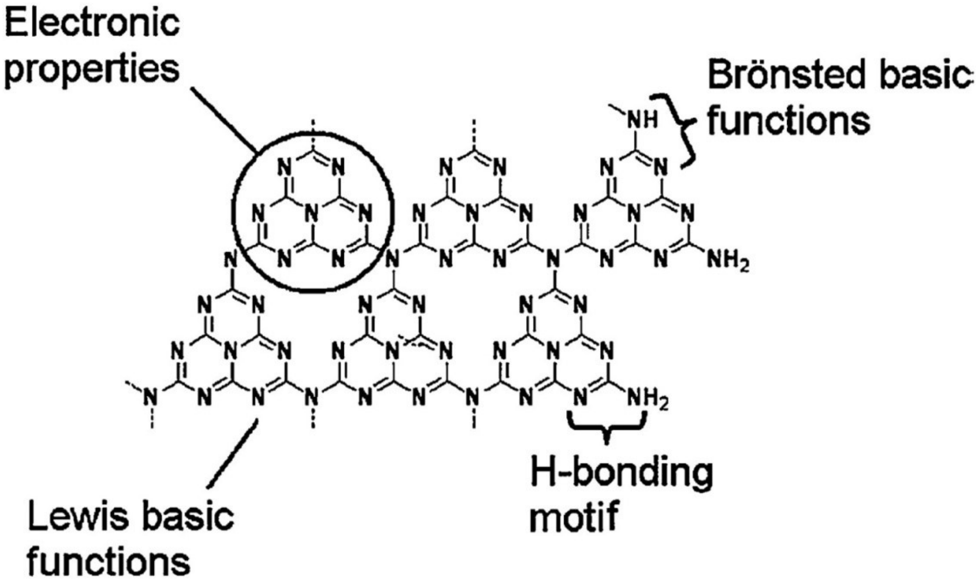

Fig. S8 Multiple functional surface properties of polymeric g-C_3N_4 material with defects.[37]

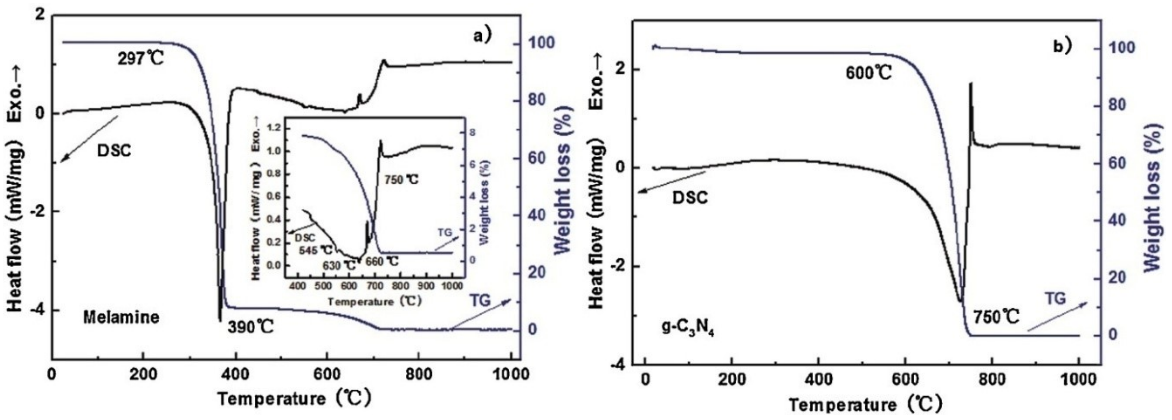

Fig. S9 The TG-DSC analysis for heating the melamine (a) and the g-C_3N_4 (b) obtained by heat polymerization of melamine at 520 °C.[82]

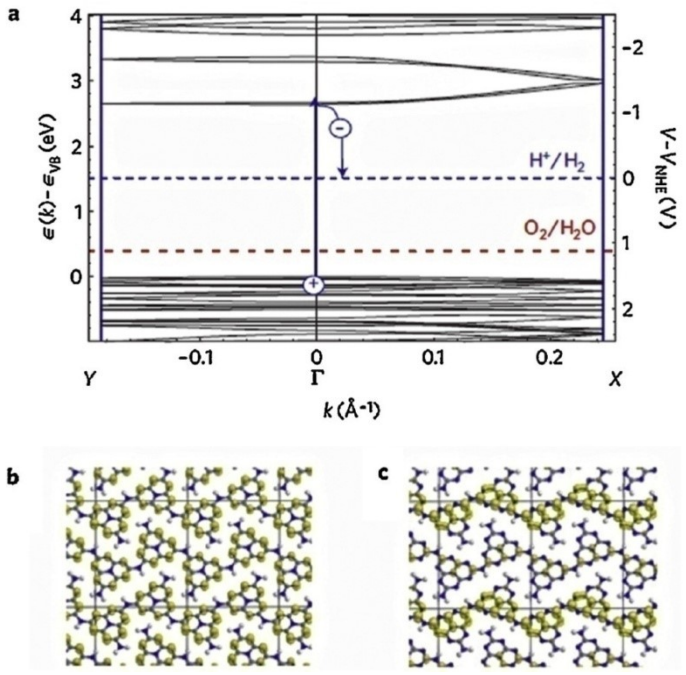

Fig. S10 Electronic structure of g-C_3N_4, (a) DFT band structure for g-C_3N_4 calculated along the Γ–X and Y–Γ directions. The potentials for H^+ to H_2 and H_2O to O_2 are displayed by the blue and red dashed lines, respectively; the Kohn–Sham orbitals for the valence band (b) and conduction band (c) of g-C_3N_4. The C, N and H atoms are gray, blue and white, respectively. The isodensity surfaces are drawn for a charge density of 0.01qe°A^{-3}.[22]

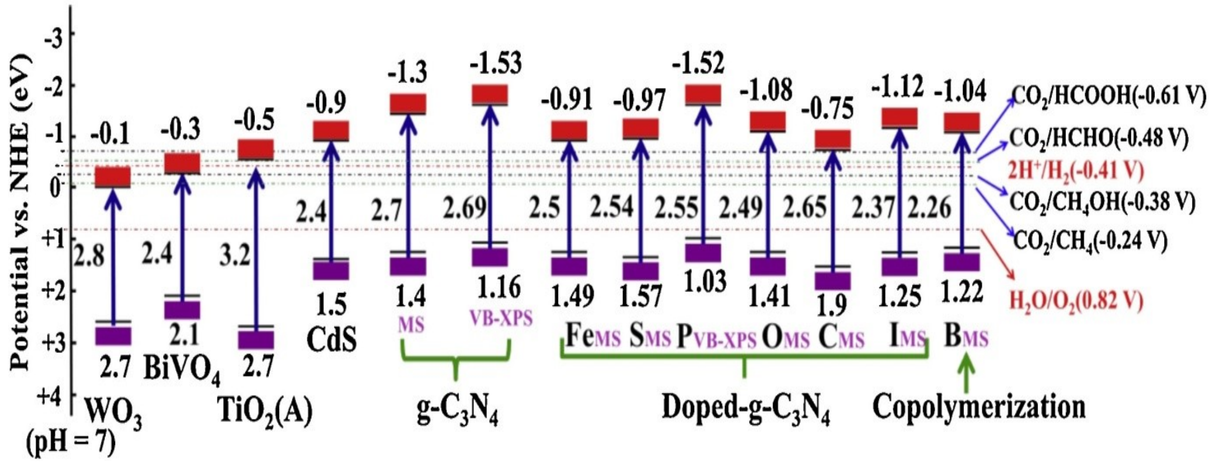

Fig. S11 Schematic illustration of the band structures of different types of g-C_3N_4 samples and other samples (VB-XPS: valence band X-ray photoelectron spectroscopy; MS: electrochemical analysis by Mott–Schottky plots).[54]

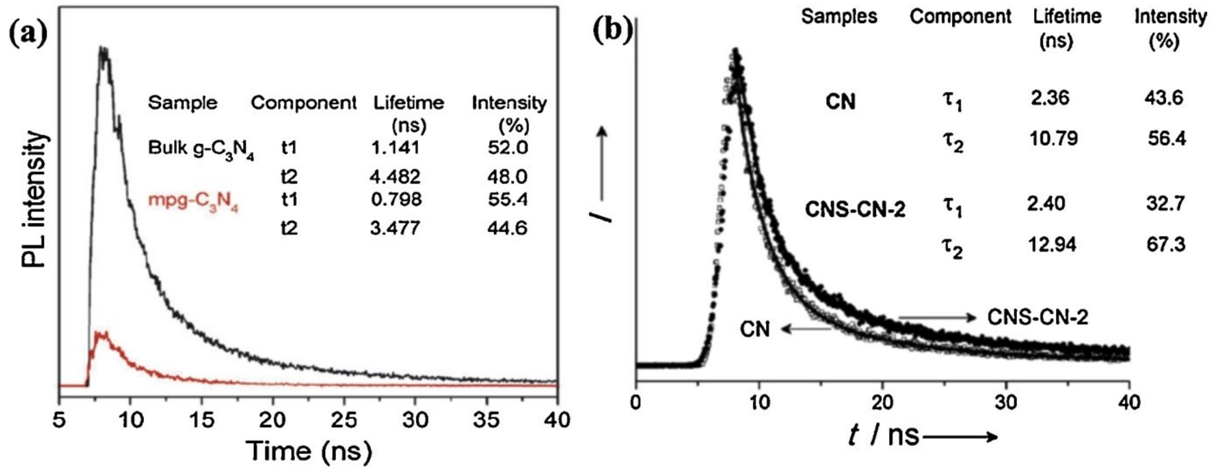

Fig. S12 (a) time-resolved PL spectrum monitored at 525 nm under 420 nm excitation at 298 K for bulk g-C_3N_4 (black) and mpg-C_3N_4 (red);[31] (b) time-resolved PL spectra monitored at 480 nm under 420 nm excitation at 77 K for CN and CNS–CN.[111]

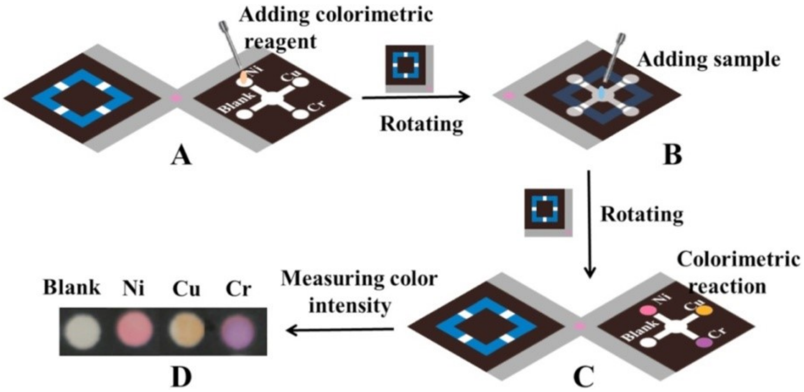

Fig. S13 Analytical procedure for the multiplexed colorimetric detection of heavy metals on the rotational paper-based device; (A) Dropping the colorimetric reagent and detection reagent into each detection zone as rotational valves were closed, (B) rotating the auxiliary layer to open valves, and adding the sample solution to the sample reservoir, (C) rotating the auxiliary layer to disconnect the detection zones with the sample reservoir, and allowing colorimetric reaction for ten minutes, (D) colorimetric detection of Ni(II), Cu(II) and Cr(VI).[139]

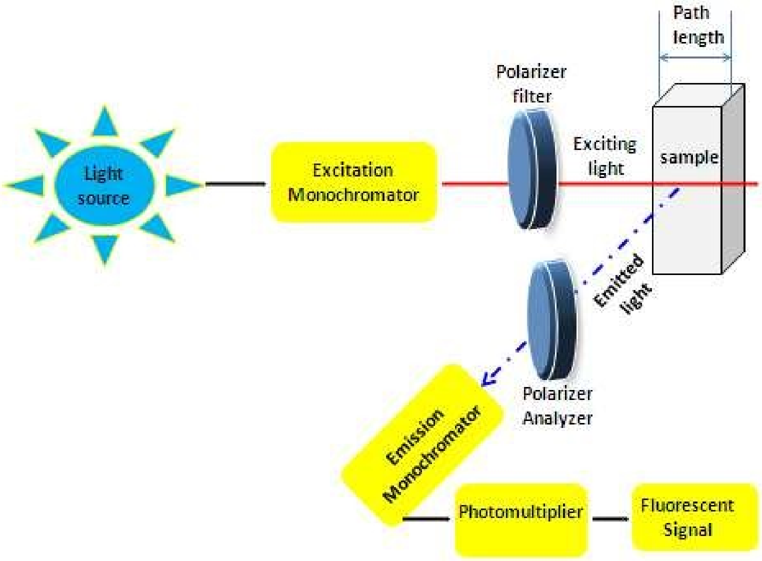

Fig. S14 Schematic representation of a fluorescence spectrophotometer.[140]

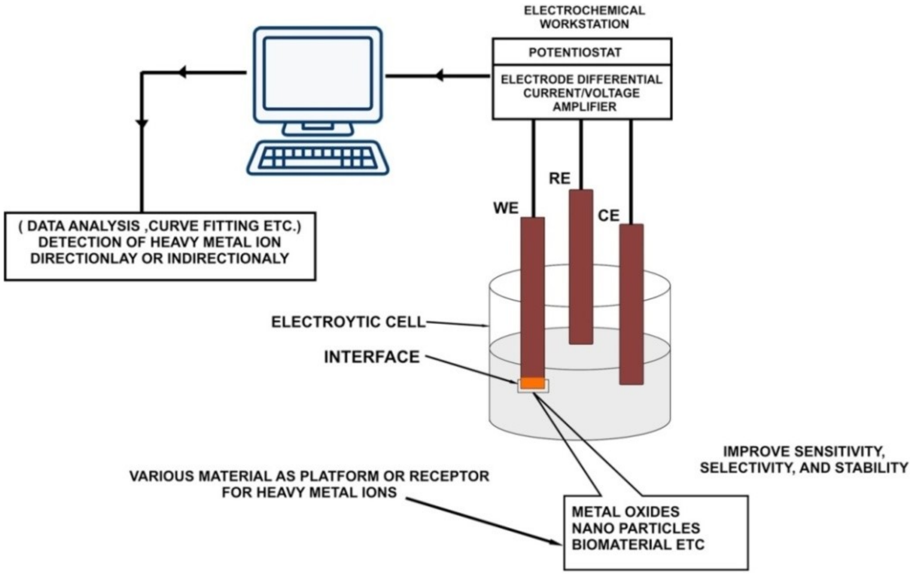

Fig. S15 General setup for electrochemical detection of heavy metal ions.[145]

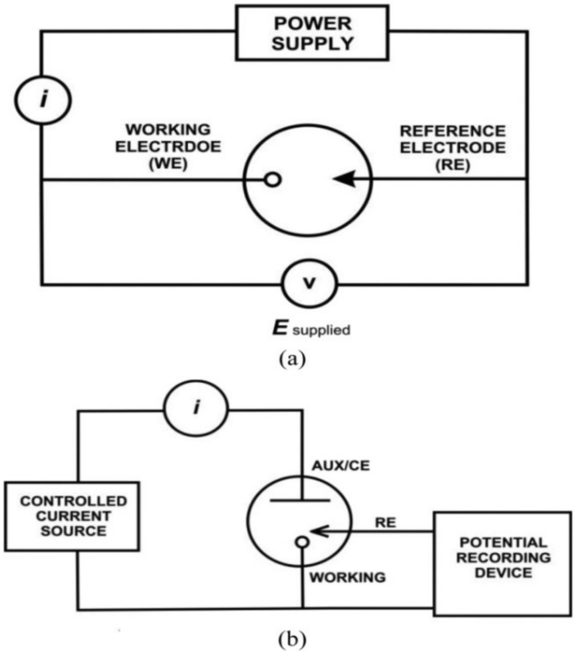

Fig. S16 (a) Two electrode cell setup and (b) three electrode cell setup.[148]

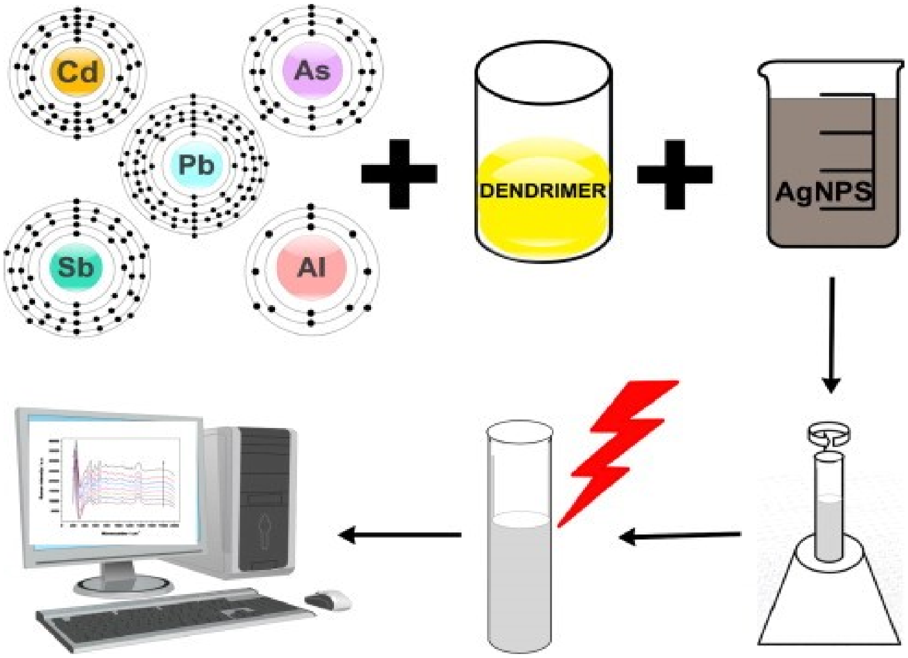

Fig. S17 Schematic illustration of experimental design.[149]

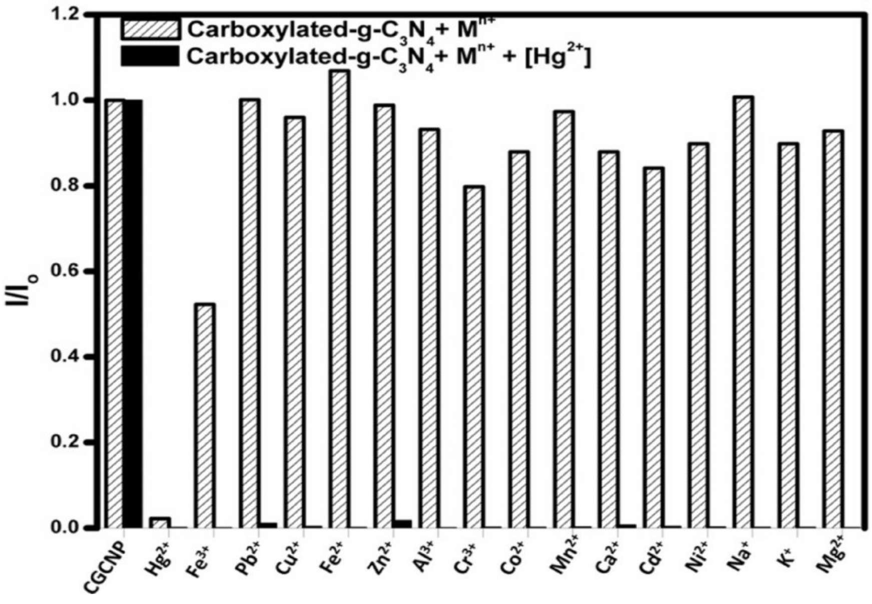

Fig. S18 Selective relative PL intensities of carboxylated-g-C_3N_4 (0.03 g L^{-1}) after treatment with 50 μM metal ion solutions (white bar), and interference of 50 μM of other metal ions with 15 μM Hg^{2+} (black bar), $\lambda_{ex} = 250$ nm.[160]

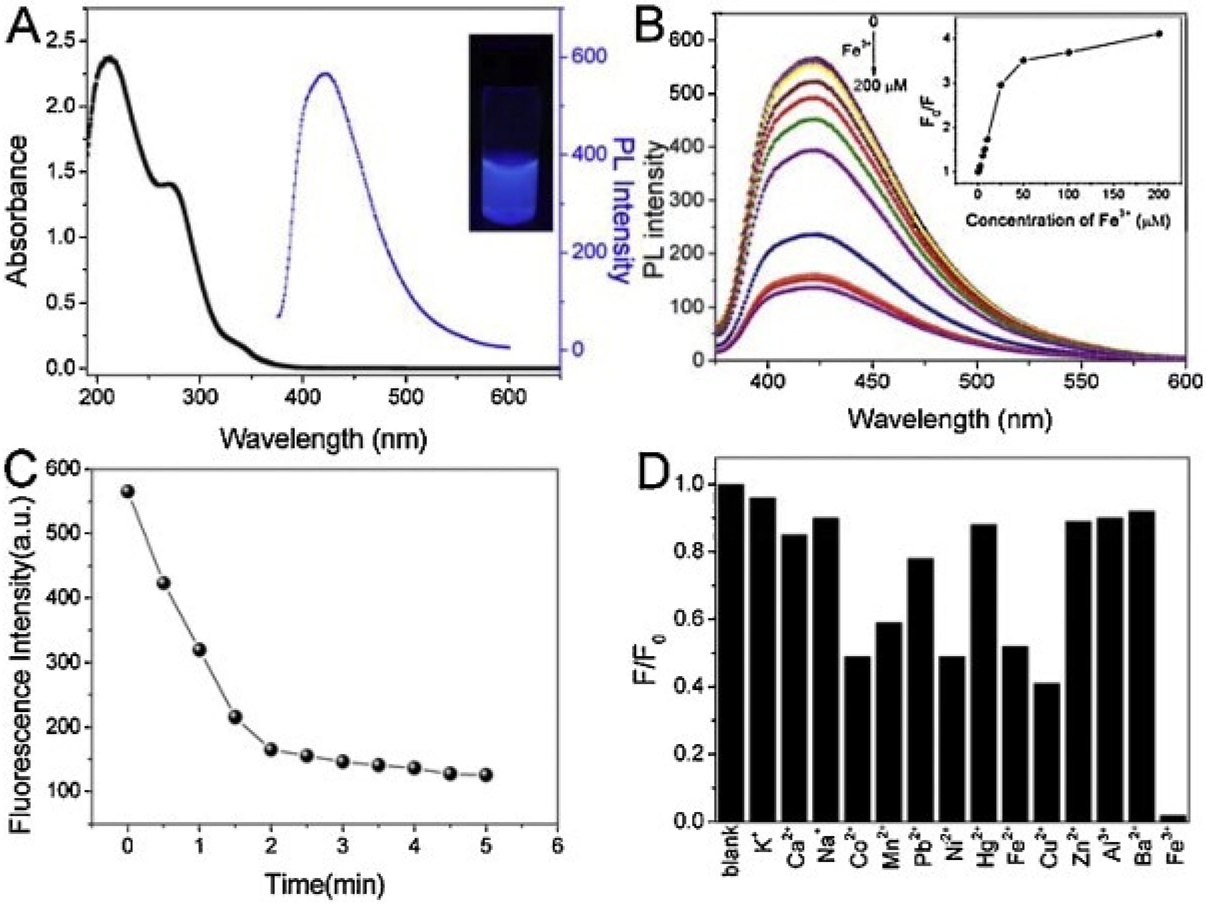

Fig. S19 (A) UV–vis absorption (black line) and PL emission (blue line) spectra of the g-C_3N_4 nanofibers thus obtained. Inset: the photograph of g-C_3N_4 nanofibers suspension under UV light (365 nm). (B) PL spectra of g-C_3N_4 nanofibers dispersion in the presence of different Fe^{3+} concentrations (from top to bottom: 0, 0.05, 0.1, 0.2, 0.5, 1, 2, 5, 7, 10, 25, 50, 100 and 200 μM). Inset: The dependent of F_0/F on the concentrations of Fe^{3+} ions within the range of 0–200 μM (excitation at 365 nm; F_0 and F are g-C_3N_4nanofibers fluorescence intensities at 425 nm in the absence and presence of Fe^{3+} ions, respectively). (C) Fluorescence quenching of g-C_3N_4 nanofibers by 200 μM Fe^{3+} in tris-HCl buffer (pH 7.4) as a function of time (λ_{ex} = 365 nm). (D) Selective PL response of g-C_3N_4 nanofibers after treatment with 1.0 mM metal ion solutions.[203]

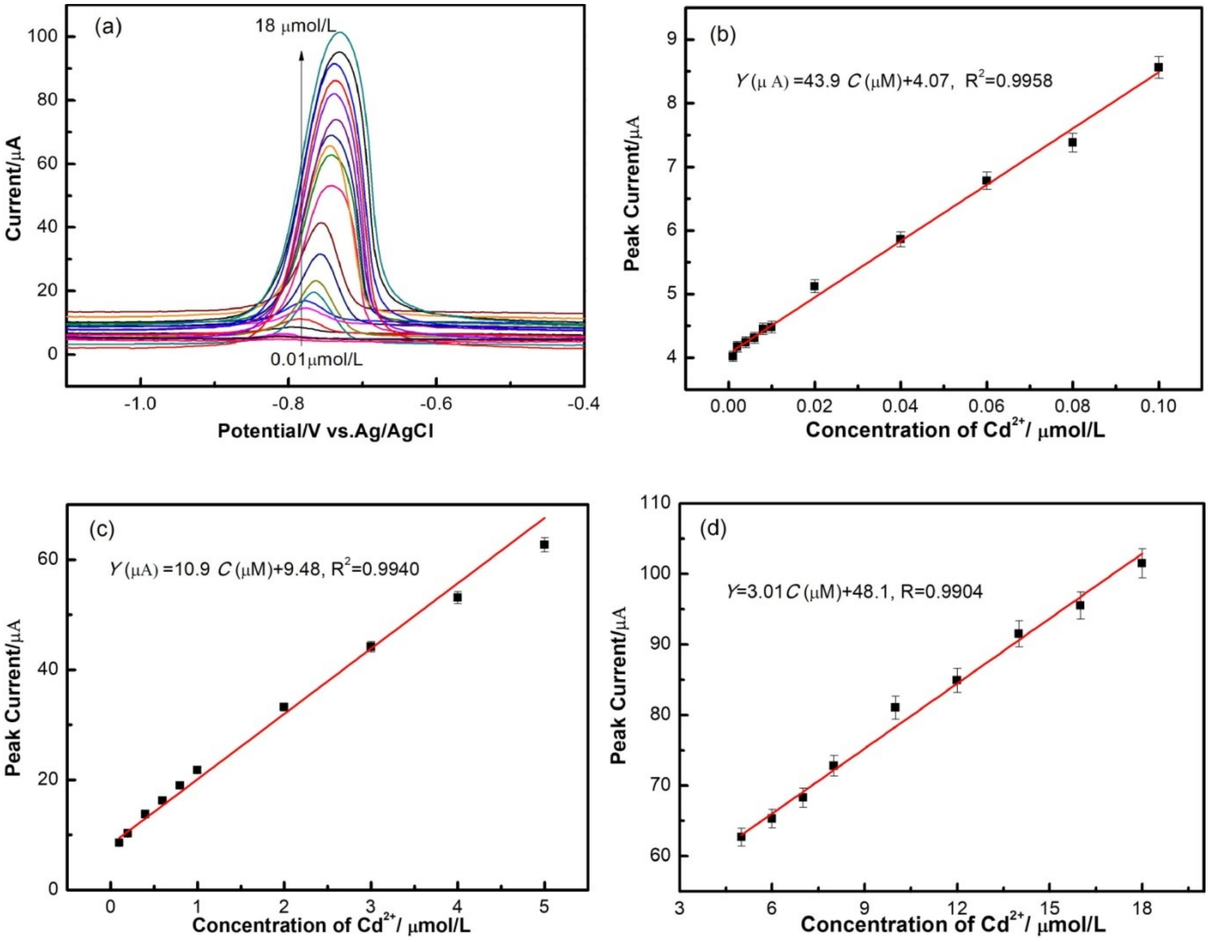

Fig. S20 (a) SWASV curves on NSCN-GC electrode in a 0.1 M HAc-NaAc buffer solution at concentrations ranging from 0.001 μM to 18 μM of Cd^{2+}, and the fitting curves of the stripping peak areas versus the concentration range of 0.001–0.1 μM (b), 0.1–5 μM (c) and 5–18 μM (d).[241]

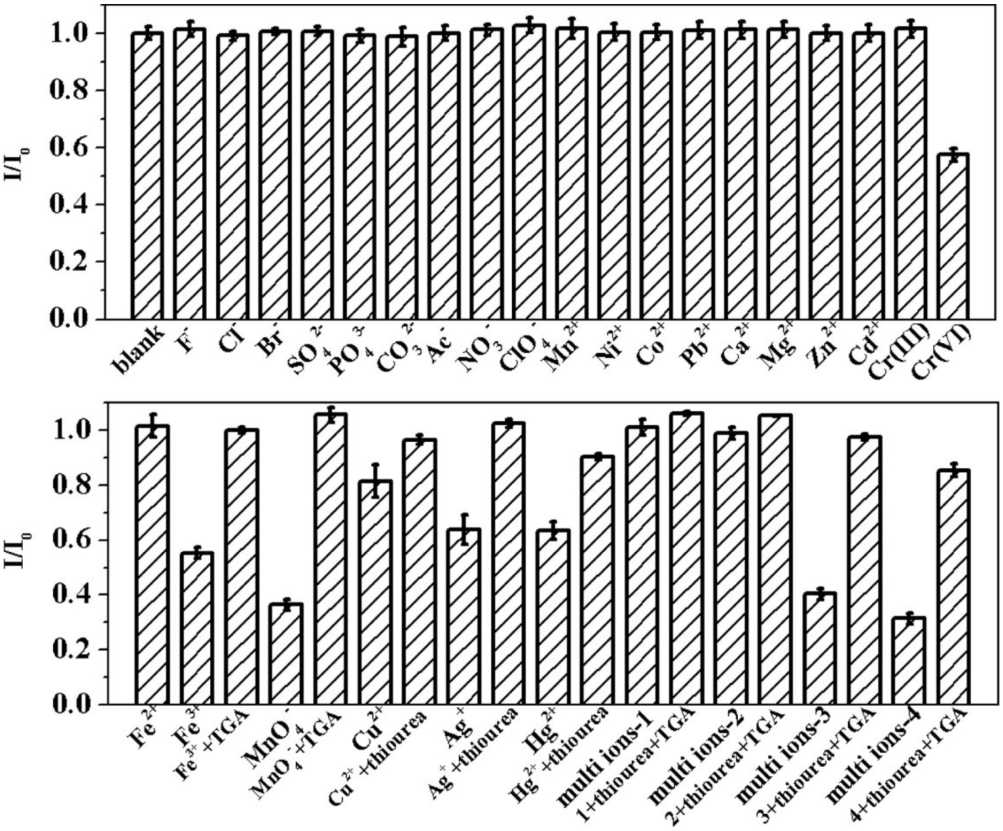

Fig. S21 Fluorescence responses of the g-C_3N_4nanosheets in the presence of 200 μM solution of various ion, The blank represents the fluorescence responses of the solution of g-C_3N_4 nanosheets without any ion, The multi-ions-1 contains Ca^{2+}, Mg^{2+}, K^+, Na^+; multi-ions-2 contains F^-, Cl^-, Br^-, SO_4^{2-}, PO_4^{3-}, CO_3^{2-}, Ac^-, NO_3^-;multi-ions-3 contains Mn^{2+}, Cu^{2+}, Ni^{2+}, Fe^{3+}, Zn^{2+}, Co^{2+}; multi-ions-4 contains Cu^{2+}, Fe^{2+}, Fe^{3+}, Hg^{2+}, the concentration of each ion in the multi-ions groups was 200 μM.[247]

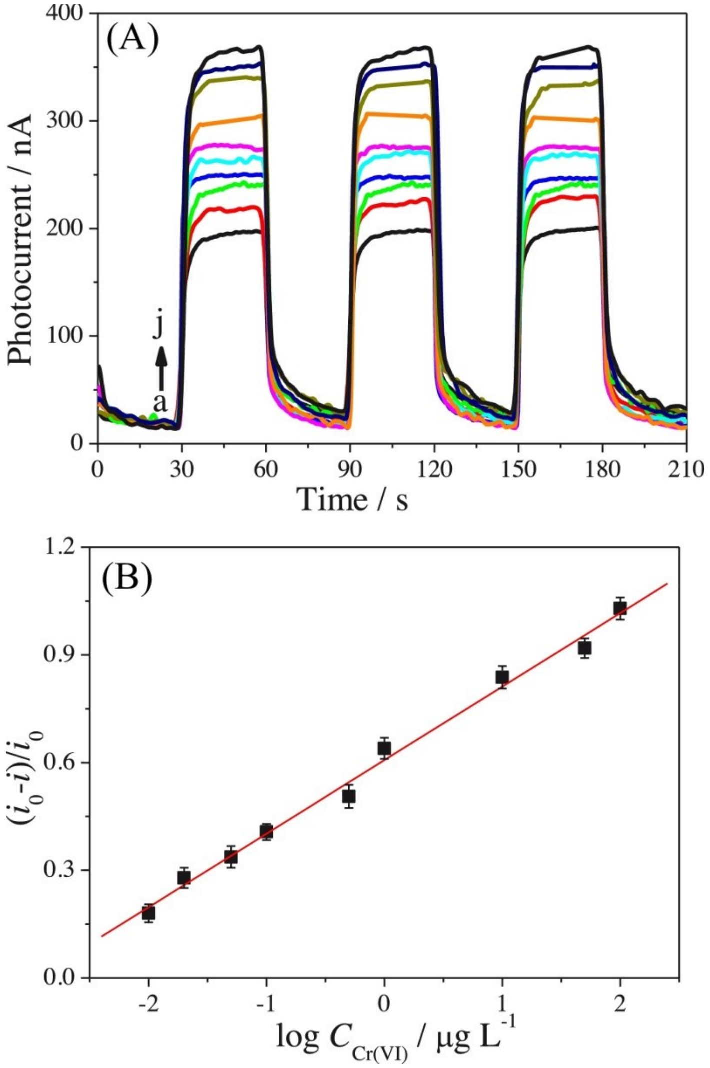

Fig. S22 (A) Photocurrent responses of IIP@F-g-C_3N_4/FTO toward Cr(VI) at increasing concentrations (from bottom to top, 0, 0.01, 0.05, 0.1, 0.5, 1.0, 10, 50 and 100 μg L^{-1}) in a supporting electrolyte of 0.1 M pH 6.0 tris–HCl, (B) Linear calibration curve.[249]

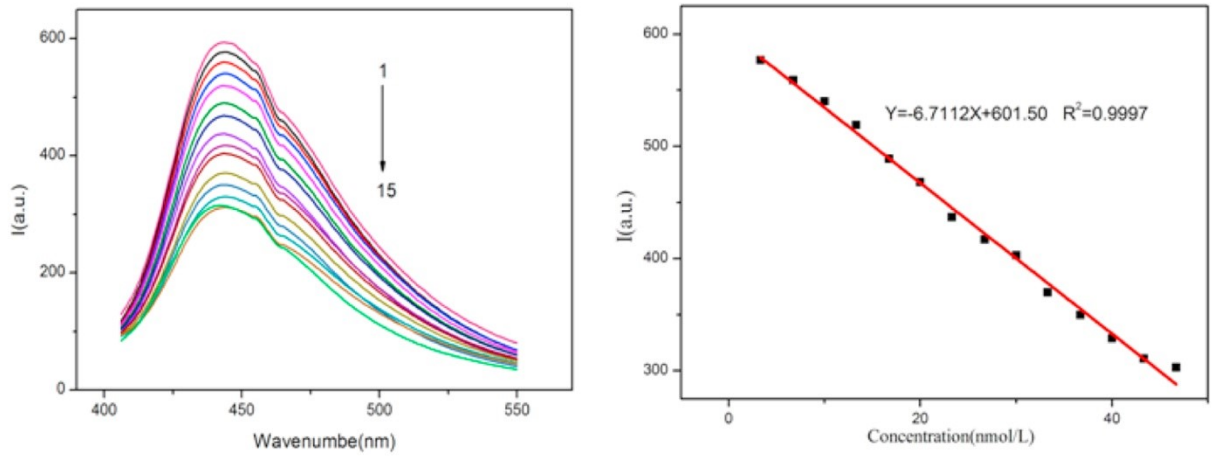

Fig. S23 Emission spectra of Ag^+ (0, 3.3., 6.7, 10, 13.3, 16.7, 20, 23.3, 26.7, 30, 33.3, 36.7, 40, 43.3, and 46.7 nM) with excitation at 310 nm (left) and the linearity of peak intensity with respect to Ag^+ concentrations (right).[265]

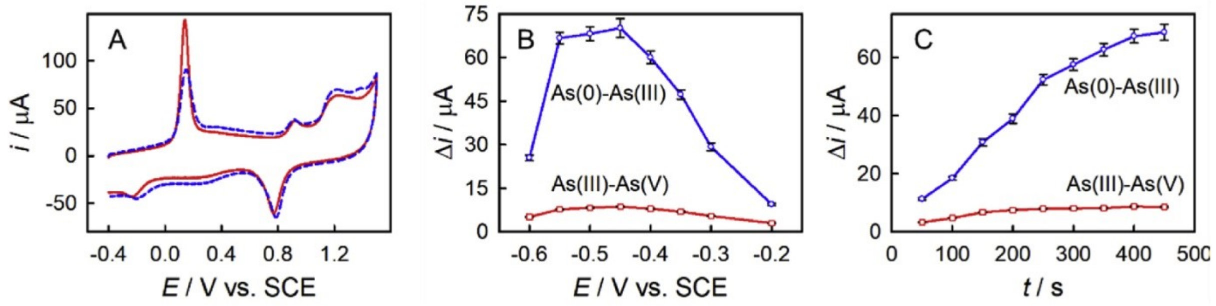

Fig. S24 (A) Cyclic voltammograms on AuNPs/GCE (dashed curve), AuNPs/g-C_3N_4/GCE (solid curve) in 0.5 M aqueous H_2SO_4 containing 2.00 μM As(III) at 1 V s^{-1}. E_{cp}: 0.4 V; tcp: 400 s, (B) Effect of E_{cp} and (C) effect of tcp on LSASV (1 V s^{-1}) peak currents of 1.00 μM As(III) in 0.5 M aqueous H_2SO_4 at AuNPs/g-C_3N_4/GCE, The LSASV experiments were conducted after preconcentration at -0.45 V for 400 s, except for the examined parameter.[281]